Coupling Finite Elements and Auxiliary Sources

D. Casati and R. Hiptmair

Coupling Finite Elements and Auxiliary Sources

D. Casati[a,*], R. Hiptmair[a]

[a]*ETH Zurich, Seminar for Applied Mathematics, Rämistrasse 101, 8092 Zurich, Switzerland*

Abstract

We consider second-order scalar elliptic boundary value problems on unbounded domains, which model, for instance, electrostatic fields. We propose a discretization that relies on a Trefftz approximation by multipole auxiliary sources in some parts of the domain and on standard mesh-based primal Lagrangian finite elements in other parts. Several approaches are developed and, based on variational saddle point theory, rigorously analyzed to couple both discretizations across the common interface:

1. Least-squares-based coupling using techniques from PDE-constrained optimization.

2. Coupling through Dirichlet-to-Neumann operators.

3. Three-field variational formulation in the spirit of mortar finite element methods.

We compare these approaches in a series of numerical experiments.

*Corresponding author
Email addresses:* `daniele.casati@sam.math.ethz.ch` (D. Casati),
`hiptmair@sam.math.ethz.ch` (R. Hiptmair)

1. Introduction

As model problem we consider the second-order scalar elliptic boundary value problem

$$- \nabla \cdot [\mathbf{A}(\mathbf{x}) \nabla u] = f \quad \text{in } \mathbb{R}^d, \ d = 2, 3, \tag{1a}$$

$$u(\mathbf{x}) = \begin{cases} c \log\|\mathbf{x}\| + \mathcal{O}(\|\mathbf{x}\|^{-1}) & \text{in } \mathbb{R}^2, \ c \in \mathbb{R}, \\ \mathcal{O}(\|\mathbf{x}\|^{-1}) & \text{in } \mathbb{R}^3 \end{cases} \quad \text{for } \|\mathbf{x}\| \to \infty \text{ uniformly,} \tag{1b}$$

where $\mathbf{A} : \mathbb{R}^d \to \mathbb{R}^{d,d}$ is a symmetric, bounded, uniformly positive-definite *diffusion coefficient*. We assume that $\mathbf{A}$ agrees with the identity matrix $\mathbf{I} \in \mathbb{R}^{d,d}$ outside of a bounded domain $\Omega_\star \subset \mathbb{R}^d$: $\mathbf{A}(\mathbf{x}) = \mathbf{I}$ for all $\mathbf{x} \in \mathbb{R}^d \setminus \Omega_\star$. In addition, $f : \mathbb{R}^d \to \mathbb{R}$ is supported in $\Omega_\star$. For the decay conditions (1b), please refer to [1, p. 259, Theorem 8.9].

Thus, the weak solution $u \in H^1_{\text{loc}}(\mathbb{R}^d)$ of (1) is harmonic in $\mathbb{R}^d \setminus \Omega_\star$, i.e. it belongs to the continuous Trefftz space

$$\mathcal{T}(\mathcal{D}) := \Big\{ v \in H^1_{\text{loc}}(\mathcal{D}) : \ \triangle v = 0,$$
$$v \text{ satisfies decay conditions (1b) if } \mathcal{D} \text{ is unbounded} \Big\} \tag{2}$$

for $\mathcal{D} = \mathbb{R}^d \setminus \Omega_\star$.

Trefftz methods seek to approximate u on subdomains of $\mathbb{R}^d \setminus \Omega_\star$ by means of some finite-dimensional subspace of $\mathcal{T}(\mathcal{D})$. Our method uses spaces spanned by potentials spawned by external multipole sources. We refer to them as the MMP approximation after the Trefftz method known as Multiple Multipole Program; see section 2 for details.

However, functions in a Trefftz space cannot approximate u in $\Omega_\star$. There we use a standard finite element space V_n, $V_n|_{\Omega_\star} \subset H^1(\Omega_\star)$, together with the usual primal variational formulation of (1).

The two linked main issues arising are 1. the principle governing the selection of the MMP approximant and 2. the coupling between the MMP domain and the Finite Element (FE) domain. Several options will be proposed and discussed in section 3.

---

[0] *Abbreviations.* FEM: Finite Element Method. MMP: Multiple Multipole Program. Index f in formulas: FEM. Index m in formulas: MMP. MAS: Method of Auxiliary Sources. PDE: Partial Differential Equation. DtN: Dirichlet-to-Neumann.

1.1. Related Work

Trefftz methods for elliptic boundary value problems have a venerable history. Specifically, Methods of Auxiliary Sources (MAS), of which MMP is an example; see [2, 3] for comprehensive surveys.

Algorithm development of MAS has been pursued by groups worldwide, for instance in Georgia (group of R. Zaridse), UK [4], Greece [5, 6], Japan [7, 8, 9], Russia [10], and also at ETH Zurich (see section 2). Most simulations reported in the literature tackle dimensionally reduced 2D models (translational or rotational symmetry, Poisson's or Helmholtz equation), but full 3D computations are becoming more common.

MAS coefficients are generally computed by least-squares or weighted residual methods, which simply enforce (weak) continuity and boundary conditions irrespectively of the considered PDE. On the other hand, Discontinuos Galerkin formulations for Trefftz methods arrive at a local variational formulation by applying integration by parts to the PDE, similarly to FEM. Together with A. Moiola and I. Perugia, the second author established a complete and rigorous convergence theory for the class of Discontinuos Galerkin Trefftz methods for both acoustic and electromagnetic scattering [11, 12, 13, 14, 15].

Concerning accuracy, it is universally reported that MAS achieves exponential convergence, provided that 1. the solution is smooth and possesses an analytic extension, and 2. both the curve Σ where the Trefftz functions are disposed and (adaptive) quadrature rules are chosen judiciously (see section 2.2 and [16, 17, 9]). However, in case of nonanalytic boundaries Γ of the MAS domain or nonsmooth data, it may not be possible to find an analytic extension of the solution beyond Γ at all. In 2D, this can be remedied by including special corner singular functions in the representation formula, see [17], or by letting Γ jut towards the corner [5, Section 4].

The ill-conditioning resulting from MAS augmentation, though inevitable, remains manageable [16]. In fact, MAS linear systems are usually ill-conditioned, something that can drastically reduce the accuracy. However, there exists a numerical algorithm that allows to obtain errors close to machine precision for the Helmholtz equation by performing a suitable change of basis [18].

Yet, there is no rigorous mathematical guidance for finding suitable curves Σ in 3D, especially if Γ features corners. For simple and canonical geometries, good choices can be made based on heuristics and experience, but this severely limits the applicability of pure MAS in 3D.

3

At the same time, little work has been devoted to the investigation of methods combining MAS with conventional finite element methods. To the best of our knowledge, this coupling has only been tackled from an engineering perspective.

Recently, J. Smajic, Ch. Hafner, and collaborators have demonstrated a simple methodology for FEM–MMP coupling at the level of 2D nonlinear magnetostatic analysis in [19]. Coupling is done by ad-hoc point matching of field values, the Dirichlet data, on the interface between the FEM and MMP domains (*collocation method*), while the Neumann data enter through a boundary term of the variational formulation. The resulting overdetermined FEM–MMP system of equations is solved in the least-squares sense.

1.2. Novelty & Outline

The authors are not aware of any prior work discussing the coupling of FEM and MAS from the perspective of numerical analysis. The approaches we propose to realize the coupling are described here for the first time.

After section 2 on MMP, the specific MAS employed in our work, in section 3 we illustrate the coupling approaches with details on their well-posedness and numerical stability. Numerical experiments are included in section 4, followed by some conclusive remarks (section 5).

2. MMP Trefftz Spaces

The concept of the Multiple Multipole Program was proposed by Ch. Hafner in his dissertation [20] based on the much older work of G. Mie and I. N. Vekua [21, 22]. Essentially, the Mie-Vekua approach expands the field in a 2D multiply connected domain by a multipole expansion (see section 2.1) supplemented with some generalized harmonic polynomials (Bessel functions). Extending these ideas, MMP introduces more multipoles (multiple multipoles) than required according to Vekua's theorems [22].

2.1. Multipoles

Basis functions spanning the MMP Trefftz spaces (2) are the so-called *multipoles*, potentials spawned by (anisotropic) point sources. This is why MMP belongs to the class of Methods of Auxiliary Sources (section 1.1). Given (2), multipoles are exact solutions of the homogeneous PDE $\triangle u = 0$ subject to the decay conditions (1b).

(a) $v_{00} = \log \rho$ (b) $v_{20} = \rho^{-2} \cos(2\theta)$ (c) $v_{30} = \rho^{-3} \cos(3\theta)$
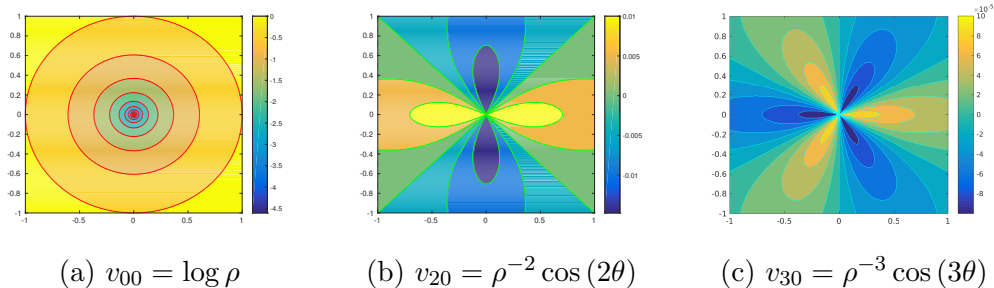
Figure 1: Sample multipoles of (3), i.e. basis functions of the 2D MMP Trefftz space (2).

A multipole can be formulated as $v(\mathbf{x}) := f(r_{xc}) g(\theta_{xc})$ or $v(\mathbf{x}) := f(r_{xc}) g(\theta_{xc}, \varphi_{xc})$ in a polar/spherical coordinate system in $\mathbb{R}^2/\mathbb{R}^3$ ($r \in [0, \infty)$, $\theta \in [0, 2\pi)$, $\varphi \in [0, \pi]$), with respect to its center $\mathbf{c} \in \mathbb{R}^d$, $d = 2, 3$. Here, $(r_{xc}, \theta_{xc}, \varphi_{xc})^\top$ are coordinates of the vector $\mathbf{x}_c := \mathbf{x} - \mathbf{c}$.

The radial dependence $f(r_{xc})$ includes a singularity at the center, $|f(r)| \to \infty$ for $r \to 0$, and the desired decay condition at infinity. Because of the singularity, multipoles must always be centered outside of the domain where they are used as a tool for approximation.

The spherical dependence $g(\theta_{xc}, \varphi_{xc})$ is generally formulated in terms of spherical harmonics [1, p. 250].

Specific multipoles chosen for our numerical experiments are:

$$\text{In } \mathbb{R}^2 : \quad \begin{cases} v_{00}(r_{xc}, \theta_{xc}) &= \log r_{xc} \\ v_{l0}(r_{xc}, \theta_{xc}) &= r_{xc}^{-l} \cos(l\theta_{xc}), \quad l = 1, \ldots, \infty \\ v_{l1}(r_{xc}, \theta_{xc}) &= r_{xc}^{-l} \sin(l\theta_{xc}), \quad l = 1, \ldots, \infty \end{cases} \quad (3)$$

These multipoles are used for the numerical experiments of sections 4.1 and 4.2. They satisfy the decay condition (1b) [1, p. 259, Theorem 8.9]. Figure 1 shows three sample multipoles from (3) with center $\mathbf{c} = \mathbf{0}$.

$$\text{In } \mathbb{R}^3 : \quad v_{lm}(r_{xc}, \theta_{xc}, \varphi_{xc}) = r_{xc}^{-l-1} Y_{lm}(\theta_{xc}, \varphi_{xc}), \quad \begin{aligned} l &= 0, \ldots, \infty \\ m &= -l, \ldots, l \end{aligned} \quad (4)$$

Here, $Y_{lm}(\theta, \varphi)$ are spherical harmonics [1, p. 250].

These multipoles are used for the numerical experiment of section 4.3. They also comply with (1b) [1, p. 259, Theorem 8.9].

5

Each multipole is characterized by a location, i.e. its center $\mathbf{c}$, and the (degree) parameters l and m. As a matter of fact, in our convergence tests we always place several multipoles at a given location up to a certain order, which is the maximum degree of multipoles with that center. Hence, we use the term *multipole expansion* when referring to several multipoles in one point up to a certain order, which is the degree where the expansion is truncated.

The total number of multipoles used for approximation is added to the total number of degrees of freedom of the discretization.

2.2. Approximation Properties

If the solution u of the 2-dimensional equation (1) possesses an analytic extension beyond the MMP domain $\Omega_{\mathrm{m}} \in \mathbb{R}^2$, into the region of $\Omega_{\mathrm{m}}^{\mathsf{c}} := \mathbb{R}^2 \setminus \Omega_{\mathrm{m}}$ between $\Gamma := \partial\Omega_{\mathrm{m}}$ and the curve Σ along which the multipole expansions are placed, then the convergence is exponential in terms of the number of degrees of freedom. This result has been proven in [9, p. 1385, Theorem 4.1] for the dipole simulation method, but the author of [9] expects that the proof can be extended to MMP [9, p. 1392, Section 6].

Moreover, we can prove that convergence results in H^1-seminorm for harmonic polynomials inside a domain $\Omega_\star \in \mathbb{R}^2$ also hold for multipoles in the complement $\Omega_\star^{\mathsf{c}} := \mathbb{R}^2 \setminus \Omega_\star$.

Proposition 1. *Let $d = 2$. If the solution $u : \Omega_\star^{\mathsf{c}} \to \mathbb{R}$*

- *is harmonic in the complement $\Omega_\star^{\mathsf{c}}$ of a 2D bounded uniformly star-shaped [23, p. 56, Assumption 3.1.1] (w.r.t. the origin) domain $\Omega_\star$,*

- *satisfies the decay condition (1b) at infinity,*

- *and possesses a harmonic extension into the domain $\Omega_\star$,*

then its best approximation by multipoles located in the origin converges exponentially with respect to the order of the multipole expansion in the H^1-seminorm.

Proof. The proof is based on Kelvin transforms [1, p. 259, Equation 8.30]:

$$u \to \mathbf{\Phi}^* u \ \text{ with } \ (\mathbf{\Phi}^* u)(\mathbf{x}) := u(\mathbf{\Phi}(\mathbf{x})), \ \mathbf{\Phi}(\mathbf{x}) := \frac{\mathbf{x}}{\|\mathbf{x}\|^2}, \ \mathbf{x} \in \mathbb{R}^2 \setminus \{\mathbf{0}\}. \quad (5)$$

For the H^1-seminorm we can show that, $\forall u : \mathcal{D} \in \mathbb{R}^2 \to \mathbb{R}$,

$$|u|_{H^1(\mathbf{\Phi}(\mathcal{D}))} = |\mathbf{\Phi}^* u|_{H^1(\mathcal{D})} \iff |u|_{H^1(\mathcal{D})} = |\mathbf{\Phi}^* u|_{H^1(\mathbf{\Phi}(\mathcal{D}))}. \quad (6)$$

When the Kelvin transform is applied to harmonic polynomials $p(r, \theta) = r^l \operatorname{cs}(l\theta)$, with r, θ polar coordinates, $l \in \mathbb{Z}^*$, $\operatorname{cs} \in \{\cos, \sin\}$, we obtain multipoles:

$$(\Phi^* p)(r, \theta) = r^{-l} \operatorname{cs}(l\theta) . \tag{7}$$

Let us now consider a solution u respecting the conditions stated above and the domain $\Omega_{\mathrm{m}} := \Omega_\star^{\mathsf{c}}$ where we want to estimate the MMP approximation.

We first define $\tilde{u} := u - c \log r$, $c \in \mathbb{R}$, whose decay condition is $\tilde{u}(\mathbf{x}) = \mathcal{O}(\|\mathbf{x}\|^{-1})$ for $\|\mathbf{x}\| \to \infty$ uniformly. Under the Kelvin transform, $\Phi^* \tilde{u} = \mathcal{O}(\|\mathbf{x}\|)$ for $\|\mathbf{x}\| \to 0$.

Given that $\Phi(\Omega_{\mathrm{m}})$ contains the unit disk and $\Phi^* \tilde{u}$ is harmonic in $\Phi(\Omega_{\mathrm{m}})$, which implies that $\Phi^* \tilde{u}$ possesses a harmonic extension beyond $\Phi(\Omega_{\mathrm{m}})$, we can obtain exponential convergence in H^1-seminorm for the approximation by harmomic polynomials of $\Phi^* \tilde{u}$ in $\Phi(\Omega_{\mathrm{m}})$ [23, p. 61, Remark 3.2.6]:

$$\forall p \in \mathbb{Z}^*, \quad \exists \alpha_l^{(p)}, \beta_l^{(p)} \in \mathbb{R}, \; l = 1, \ldots, p :$$
$$\left| \Phi^* \tilde{u} - \sum_{l=1}^p \alpha_l^{(p)} r^l \cos(l\theta) + \beta_l^{(p)} r^l \sin(l\theta) \right|_{H^1(\Phi(\Omega_{\mathrm{m}}))} \le C\, q^p \tag{8}$$
$$\text{for some } 0 \le q \le 1, \quad C \in \mathbb{R}^+ \text{ independent of } p .$$

By applying (6) and (7) to (8), we get that

$$\forall p \in \mathbb{Z}^*, \quad \exists \alpha_l^{(p)}, \beta_l^{(p)} \in \mathbb{R}, \; l = 1, \ldots, p :$$
$$\left| \tilde{u} - \sum_{l=1}^p \alpha_l^{(p)} r^{-l} \cos(l\theta) + \beta_l^{(p)} r^{-l} \sin(l\theta) \right|_{H^1(\Omega_{\mathrm{m}})} \le C\, q^p \tag{9}$$
$$\text{for some } 0 \le q \le 1, \quad C \in \mathbb{R}^+ \text{ independent of } p .$$

Now we can restore the proper decay condition of u, $c \log r + \mathcal{O}(\|\mathbf{x}\|^{-1})$ for $\|\mathbf{x}\| \to \infty$, where $c \in \mathbb{R}$ is given by the coefficient $\alpha_0^{(p)}$ of the zeroth-order multipole $v_{00}(r, \theta) = \log r$ (see (3)). This concludes the proof.

$\square$

A corresponding result for $d = 3$ remains elusive.

We now perform numerical experiments to illustrate these convergence results in $\mathbb{R}^2$. Ω_{m} is the complement of the unit square $[0, 1]^2$. We test the following solutions which enjoy a $\mathcal{O}(\|\mathbf{x}\|^{-1})$ decay for $\|\mathbf{x}\| \to \infty$:

1. $u(\mathbf{x}) = \rho_{xc}^{-2} \sin(2\theta_{xc})$, where $r_{xc} \in [0, \infty)$ and $\theta_{xc} \in [0, 2\pi)$ are polar coordinates of vector $\mathbf{x} - \mathbf{c}$, $\mathbf{c} = (0.4, 0.4)^\top$. This is a harmonic function $\in H^1(\mathbb{R}^2)$ that uniformly decays for $\|\mathbf{x}\| \to \infty$ with a singularity in $(0.4, 0.4)^\top$.

2. $u(\mathbf{x}) = \rho^{-2} \sin(2\theta)$. This is a harmonic function $\in H^1(\mathbb{R}^2)$ that uniformly decays for $\|\mathbf{x}\| \to \infty$ with a singularity in the origin, a corner of the boundary Γ of the unit square.

Multipoles are chosen from (3). We consider these configurations:

1. Multipole expansions up to a fixed order 1 uniformly located on a circle at the center of the unit square with radius 0.25. During the test we increase the number of expansions.
   Note that, given this choice of multipoles, the singularity of the first solution lies inside the circle of multipoles, i.e. the first solution has an analytic extension between Γ and the circle of multipoles Σ.

2. Multipoles up to a given order placed in the center of the unit square $(0.5, 0.5)^\top$. During the test we increase the order.

We compute the best approximation of the solutions in spaces spanned by multipoles by means of the collocation method on uniformly spaced points on the edges of the unit square (corners are avoided). The number of points is chosen to make the overdetermined system almost square. The system is then solved by QR decomposition.

The approximation error in H^1-seminorm is computed using

$$\int_{\Omega_m} |\nabla(u - u_m)|^2 \, d\boldsymbol{x} = \int_{\partial\Omega_m} (u - u_m) \left[\mathbf{n} \cdot \nabla(u - u_m) \right] dS \qquad (10)$$

and the integral is approximated by Gaussian quadrature.

For the first solution with an analytic extension, we observe exponential convergence given both fixed-order multipole expansions on the units circle and a variable-order expansion placed in the origin, as shown in figs. 2a and 2b, respectively. This is in accordance with Proposition 1 and the literature.

For the singular solution in the origin, we see convergence from fig. 3, but merely algebraic (and the error is much higher).
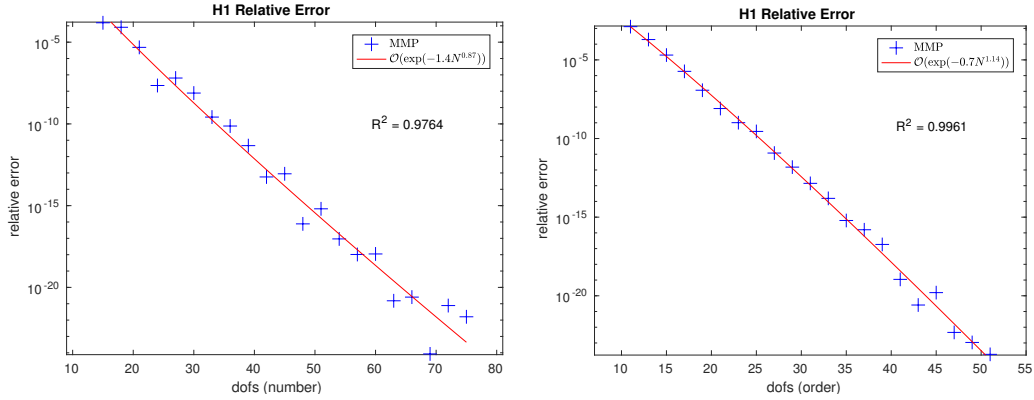
(a) Increasing number of expansions. (b) Expansion with increasing order.

Figure 2: Convergence plots of MMP for solution $\rho_{xc}^{-2} \sin\left(2\theta_{xc}\right)$, with $\mathbf{c} = \left(0.4, 0.4\right)^{\top}$. The exponential convergence curve $C \exp\left(-\gamma N^{\delta}\right)$, $C, \gamma, \delta \in \mathbb{R}$, is fitted to the data.
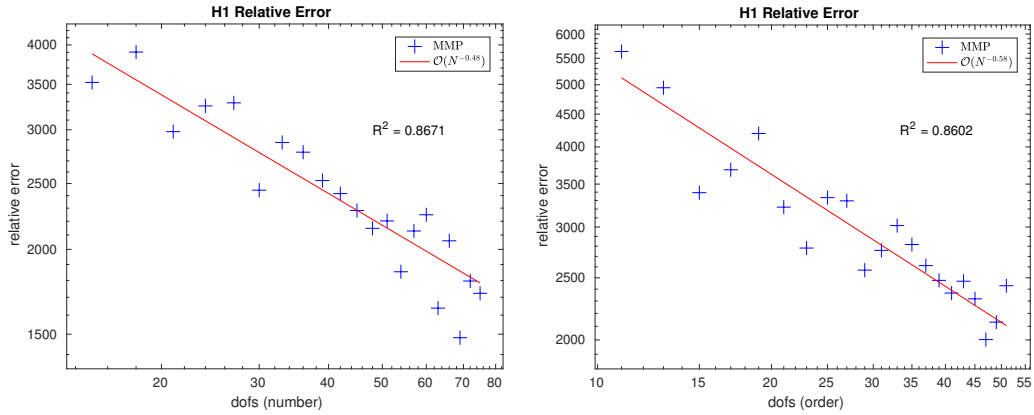
(a) Increasing number of expansions. (b) Expansion with increasing order.

Figure 3: Convergence plots of MMP for solution $\rho^{-2} \sin\left(2\varphi\right)$. The algebraic convergence curve $CN^{-\alpha}$, $C, \alpha \in \mathbb{R}$, is fitted to the data.

9

3. Coupling Strategies

We consider the partition $\mathbb{R}^d = \Omega_{\mathrm{f}} \cup \Gamma \cup \Omega_{\mathrm{m}}$, $d = 2, 3$, $\Gamma := \partial\Omega_{\mathrm{f}} = \partial\Omega_{\mathrm{m}}$, $\Omega_{\mathrm{f}} \cap \Omega_{\mathrm{m}} = \varnothing$. Ω_{f} is a bounded Lipschitz domain, the FE domain, whereas Ω_{m} is dubbed the MMP domain. The terminology indicates the type of approximation of u to be employed in the subdomain. Coupling is done across the interface Γ. We demand $\Omega_\star \subset \Omega_{\mathrm{f}}$, but not necessarily $\Omega_\star = \Omega_{\mathrm{f}}$. If $\Omega_\star \neq \Omega_{\mathrm{f}}$, Γ is an artificial interface. We define

$$u^{\mathrm{f}} := u|_{\Omega_{\mathrm{f}}} \in H^1(\Omega_{\mathrm{f}}) \ , \quad u^{\mathrm{m}} := u|_{\Omega_{\mathrm{m}}} \in H^1_{\mathrm{loc}}(\Omega_{\mathrm{m}}) \ . \tag{11}$$

As natural norms we use *energy norms*. For u^{f} defined on the bounded domain Ω_{f}, the energy norm is $\|u^{\mathrm{f}}\|_{H^1(\Omega_{\mathrm{f}})}$. For $u^{\mathrm{m}} \in \mathcal{T}(\Omega_{\mathrm{m}})$ and $d = 3$, we use $\|u^{\mathrm{m}}\|_{\mathcal{T}(\Omega_{\mathrm{m}})} := |u^{\mathrm{m}}|_{H^1(\Omega_{\mathrm{m}})} := \|\nabla u^{\mathrm{m}}\|_{L^2(\Omega_{\mathrm{m}})}$. For $d = 2$, the energy norm is not necessarily well-defined. In this case we rely on the norm

$$\|u^{\mathrm{m}}\|_{\mathcal{T}(\Omega_{\mathrm{m}})} := |c| + \|\nabla(u^{\mathrm{m}} - c\,\log\|\mathbf{x}\|)\|_{L^2(\Omega_{\mathrm{m}})} \tag{12}$$

with $c \in \mathbb{R}$, such that

$$(u^{\mathrm{m}} - c\,\log\|\mathbf{x}\|)(\mathbf{x}) = \mathcal{O}\left(\|\mathbf{x}\|^{-1}\right) \text{ for } \|\mathbf{x}\| \to \infty \ . \tag{13}$$

We denote by $\gamma_{\mathbf{n}}$ the *co-normal trace operator* $\gamma_{\mathbf{n}} : H^1_{\mathrm{loc}}(\triangle, \Omega_\circ) \to H^{-\frac{1}{2}}(\Gamma)$, $\gamma_{\mathbf{n}} v := \mathbf{n} \cdot \mathbf{A}\nabla v$, $v \in H^1_{\mathrm{loc}}(\triangle, \Omega_\circ)$, $H^1_{\mathrm{loc}}(\triangle, \Omega_\circ)$ the space of functions $v \in H^1_{\mathrm{loc}}(\Omega_\circ)$ for which $\triangle v \in L^2_{\mathrm{loc}}(\Omega_\circ)$, given $\circ = \mathrm{f}, \mathrm{m}$. We always take $\mathbf{n}$ as the normal pointing outwards with respect to Ω_{f} into Ω_{m}.

Across Γ the solution u of (1) has to satisfy the *transmission conditions* [24, p. 107, Lemma 5.3]

$$u^{\mathrm{f}}\big|_\Gamma = u^{\mathrm{m}}\big|_\Gamma \ , \tag{14a}$$

$$\gamma_{\mathbf{n}} u^{\mathrm{f}}\big|_\Gamma = \gamma_{\mathbf{n}} u^{\mathrm{m}}\big|_\Gamma \ . \tag{14b}$$

The starting point for all coupling approaches will be the weak form of (1) in Ω_{f}. By testing the PDE with $v_{\mathrm{f}} \in H^1(\Omega_{\mathrm{f}})$, integrating over Ω_{f}, and using the transmission condition (14b), after integrating by parts we obtain

$$\int_{\Omega_{\mathrm{f}}} \mathbf{A}\nabla u^{\mathrm{f}} \cdot \nabla v^{\mathrm{f}} \,\mathrm{d}\boldsymbol{x} - \int_\Gamma \gamma_{\mathbf{n}} u^{\mathrm{m}} \, v^{\mathrm{f}} \,\mathrm{d}S = \int_{\Omega_{\mathrm{f}}} f \, v^{\mathrm{f}} \,\mathrm{d}\boldsymbol{x} \quad \forall v^{\mathrm{f}} \in H^1(\Omega_{\mathrm{f}}) \ . \tag{15}$$

10

Depending on how we impose the additional interface condition (14a), we end up with different coupling approaches that lead to different *linear variational saddle point problems* to be discussed in the following sections. Throughout, we will rely on the abstract saddle point theory, as presented, for instance, in [25, Chapter III, Section 4].

3.1. PDE-constrained Least-Squares Coupling

Taking the cue from (14a), we seek $u^{\mathrm{f}} \in H^1(\Omega_{\mathrm{f}})$, $u^{\mathrm{m}} \in \mathcal{T}(\Omega_{\mathrm{m}})$,

- minimizing

$$J_\Gamma\left(u^{\mathrm{f}}, u^{\mathrm{m}}\right) := \|u^{\mathrm{f}} - u^{\mathrm{m}}\|_{L^2(\Gamma)}^2 \tag{16}$$

- and satisfying the constraint (15).

This is a quadratic minimization problem under a linear variational constraint, whose necessary and sufficient optimality conditions give rise to the following saddle point problem:

Seek $u^{\mathrm{f}} \in H^1(\Omega_{\mathrm{f}})$, $u^{\mathrm{m}} \in \mathcal{T}(\Omega_{\mathrm{m}})$, $p^{\mathrm{f}} \in H^1(\Omega_{\mathrm{f}})$:
$$\begin{cases} \mathrm{a}^{\mathrm{LS}}\left(\left(u^{\mathrm{f}}, u^{\mathrm{m}}\right), \left(v^{\mathrm{f}}, v^{\mathrm{m}}\right)\right) & + & \mathrm{b}^{\mathrm{LS}}\left(\left(v^{\mathrm{f}}, v^{\mathrm{m}}\right), p^{\mathrm{f}}\right) & = & 0 \\ \mathrm{b}^{\mathrm{LS}}\left(\left(u^{\mathrm{f}}, u^{\mathrm{m}}\right), q^{\mathrm{f}}\right) & & & = & \int_{\Omega_{\mathrm{f}}} f \, q^{\mathrm{f}} \, \mathrm{d}\boldsymbol{x} \end{cases}$$
$$\forall v^{\mathrm{f}} \in H^1(\Omega_{\mathrm{f}}), \quad \forall v^{\mathrm{m}} \in \mathcal{T}(\Omega_{\mathrm{m}}), \quad \forall q^{\mathrm{f}} \in H^1(\Omega_{\mathrm{f}}) \tag{17}$$

where

$$\mathrm{a}^{\mathrm{LS}}\left(\left(u^{\mathrm{f}}, u^{\mathrm{m}}\right), \left(v^{\mathrm{f}}, v^{\mathrm{m}}\right)\right) := \int_\Gamma \left(u^{\mathrm{f}} - u^{\mathrm{m}}\right)\left(v^{\mathrm{f}} - v^{\mathrm{m}}\right) \, \mathrm{d}S \,, \tag{18a}$$

$$\mathrm{b}^{\mathrm{LS}}\left(\left(u^{\mathrm{f}}, u^{\mathrm{m}}\right), q^{\mathrm{f}}\right) := \int_{\Omega_{\mathrm{f}}} \mathbf{A}\nabla u^{\mathrm{f}} \cdot \nabla q^{\mathrm{f}} \, \mathrm{d}\boldsymbol{x} - \int_\Gamma \gamma_{\mathbf{n}} u^{\mathrm{m}} \, q^{\mathrm{f}} \, \mathrm{d}S \,. \tag{18b}$$

The constraint implied by the second line of (17) uniquely defines a function $u^{\mathrm{f}} = u^{\mathrm{f}}(u^{\mathrm{m}})$, satisfying $\gamma_{\mathbf{n}} u^{\mathrm{f}} = \gamma_{\mathbf{n}} u^{\mathrm{m}}$ from (14b). Thus, the existence and uniqueness of a solution to (17) follows from those for (1). However, stability remains elusive without further considerations.

Remark 1. If we relied on the $H^{\frac{1}{2}}(\Gamma)$-inner product $\langle \cdot, \cdot \rangle_{H^{\frac{1}{2}}(\Gamma)}$ and defined

$$a^{\mathrm{LS}}\left(\left(u^{\mathrm{f}}, u^{\mathrm{m}}\right), \left(v^{\mathrm{f}}, v^{\mathrm{m}}\right)\right) := \langle u^{\mathrm{f}} - u^{\mathrm{m}}, \, v^{\mathrm{f}} - v^{\mathrm{m}} \rangle_{H^{\frac{1}{2}}(\Gamma)}, \qquad (19)$$

then the *ellipticity on the kernel* condition of abstract saddle point theory would be satisfied for (17). To see it note that, if $\left(u^{\mathrm{f}}, u^{\mathrm{m}}\right) \in H^1(\Omega_{\mathrm{f}}) \times \mathcal{T}(\Omega_{\mathrm{m}})$ satisfy $\mathrm{b}^{\mathrm{LS}}\left(\left(u^{\mathrm{f}}, u^{\mathrm{m}}\right), q^{\mathrm{f}}\right) = 0$ for all $q^{\mathrm{f}} \in H^1(\Omega_{\mathrm{f}})$, then integration by parts in Ω_{m} shows

$$|u^{\mathrm{f}}|^2_{H^1(\Omega_{\mathrm{f}})} + |u^{\mathrm{m}}|^2_{H^1(\Omega_{\mathrm{m}})} \leq C \left\{ \|u^{\mathrm{f}} - u^{\mathrm{m}}\|^2_{H^{\frac{1}{2}}(\Gamma)} + \|\gamma_{\mathbf{n}} u^{\mathrm{f}} - \gamma_{\mathbf{n}} u^{\mathrm{m}}\|^2_{H^{-\frac{1}{2}}(\Gamma)} \right\} \quad (20)$$

for some $C \in \mathbb{R}^+$. The second term on the right-hand side vanishes. Yet, the $H^{\frac{1}{2}}(\Gamma)$-inner product is nonlocal and, consequently, not suitable for numerical purposes.

The Galerkin discretization of (17) is straightforward:

1. We replace $H^1(\Omega_{\mathrm{f}})$ with a Lagrangian finite element space V_n built on a mesh of Ω_{f}.

2. We approximate u^{m} and v^{m} in a finite-dimensional Trefftz space $\mathcal{T}_n \subset \mathcal{T}(\Omega_{\mathrm{m}})$.

We appeal to variational saddle point theory and note that a uniform discrete *inf-sup condition* of abstract saddle point theory for b^{LS} is immediate.

On the other hand, ellipticity on the discrete kernel

$$\ker_n \mathrm{b}^{\mathrm{LS}} := \left\{ \left(v^{\mathrm{f}}_n, v^{\mathrm{m}}_n\right) \in V_n \times \mathcal{T}_n : \mathrm{b}^{\mathrm{LS}}\left(\left(v^{\mathrm{f}}, v^{\mathrm{m}}\right), q^{\mathrm{f}}\right) = 0 \quad \forall q^{\mathrm{f}} \in V_n \right\} \quad (21)$$

hinges on an inverse inequality. Define

$$K_n := \sup \left\{ \|\gamma_{\mathbf{n}} u^{\mathrm{m}}_n\|_{L^2(\Gamma)}, \, \|\gamma_{\mathbf{n}} u^{\mathrm{m}}_n\|_{H^{-\frac{1}{2}}(\Gamma)} \right\}, \qquad (22)$$

where $\|\gamma_{\mathbf{n}} u^{\mathrm{m}}_n\|_{H^{-\frac{1}{2}}(\Gamma)} = 1$ for $u^{\mathrm{m}}_n \in \mathcal{T}_n$.

By the equivalence of all norms on finite dimensional spaces, a finite $K_n \in \mathbb{R}^+$ will exist. Let $\left(u^{\mathrm{f}}_n, u^{\mathrm{m}}_n\right) \in \ker_n \mathrm{b}^{\mathrm{LS}}$. This means that $\int_\Gamma \gamma_{\mathbf{n}} u^{\mathrm{m}}_n \, \mathrm{d}S = 0$,

12

which implies $\nabla u_n^{\mathrm{m}}(\mathbf{x}) = \mathcal{O}\left(\|\mathbf{x}\|^{-2}\right)$. As a consequence, $\nabla u_n^{\mathrm{m}} \in L^2(\Omega_{\mathrm{m}})$ also for $d = 2$. Thus, we get

$$\int_{\Omega_{\mathrm{f}}} \mathbf{A} \nabla u_n^{\mathrm{f}} \cdot \nabla u_n^{\mathrm{f}} \, \mathrm{d}\boldsymbol{x} + \int_{\Omega_{\mathrm{m}}} \|\nabla u_n^{\mathrm{m}}\|^2 \, \mathrm{d}\boldsymbol{x} = \int_{\Gamma} \left(u_n^{\mathrm{f}} - u_n^{\mathrm{m}}\right) \gamma_{\mathbf{n}} u_n^{\mathrm{m}} \, \mathrm{d}S \, . \qquad (23)$$

We conclude that, with $C \in \mathbb{R}^+$ independent of the choice of both V_n and $\mathcal{T}_n$,

$$\|\nabla u_n^{\mathrm{f}}\|_{L^2(\Omega_{\mathrm{f}})}^2 + \|\nabla u_n^{\mathrm{m}}\|_{L^2(\Omega_{\mathrm{m}})}^2 \leq C \|u_n^{\mathrm{f}} - u_n^{\mathrm{m}}\|_{L^2(\Gamma)} \cdot \|\gamma_{\mathbf{n}} u_n^{\mathrm{m}}\|_{L^2(\Gamma)} \, . \qquad (24)$$

Next, we use the inverse inequality implicit in (22) together with the estimate $\|\gamma_{\mathbf{n}} u^{\mathrm{m}}\|_{H^{-\frac{1}{2}}(\Gamma)} \leq C \|\nabla u^{\mathrm{m}}\|_{L^2(\Omega_{\mathrm{m}})} \quad \forall u^{\mathrm{m}} \in \mathcal{T}(\Omega_{\mathrm{m}}), \ C \in \mathbb{R}^+$, and obtain

$$\|\nabla u_n^{\mathrm{f}}\|_{L^2(\Omega_{\mathrm{f}})} + \|\nabla u_n^{\mathrm{m}}\|_{L^2(\Omega_{\mathrm{m}})} \leq C K_n \|u_n^{\mathrm{f}} - u_n^{\mathrm{m}}\|_{L^2(\Gamma)} \, , \qquad (25)$$

which proves the ellipticity of a^{LS} on $\ker_n \mathrm{b}^{\mathrm{LS}}$, albeit with a constant K_n tending to zero as the Trefftz space $\mathcal{T}_n$ is refined. Hence, the discrete variational problem is stable, but convergence is guaranteed only if, asymptotically, the approximation errors decay faster than K_n increases.

3.2. Dirichlet-to-Neumann-based Coupling

We take into account the continuity transmission condition (14a) in weak form, testing it with co-normal traces $\gamma_{\mathbf{n}} v^{\mathrm{m}}$ of $v^{\mathrm{m}} \in \mathcal{T}(\Omega_{\mathrm{m}})$:

$$\int_{\Gamma} u^{\mathrm{f}} \gamma_{\mathbf{n}} v^{\mathrm{m}} \, \mathrm{d}S - \int_{\Gamma} u^{\mathrm{m}} \gamma_{\mathbf{n}} v^{\mathrm{m}} \, \mathrm{d}S = 0 \qquad \forall v^{\mathrm{m}} \in \mathcal{T}(\Omega_{\mathrm{m}}) \, . \qquad (26)$$

Combining (26) with the variational form of (15), we end up with:

Seek $u^{\mathrm{f}} \in H^1(\Omega_{\mathrm{f}}), \ u^{\mathrm{m}} \in \mathcal{T}(\Omega_{\mathrm{m}})$:

$$\begin{cases} \int_{\Omega_{\mathrm{f}}} \mathbf{A} \nabla u^{\mathrm{f}} \cdot \nabla v^{\mathrm{f}} \, \mathrm{d}\boldsymbol{x} & - & \int_{\Gamma} \gamma_{\mathbf{n}} u^{\mathrm{m}} \, v^{\mathrm{f}} \, \mathrm{d}S & = & \int_{\Omega_{\mathrm{f}}} f \, v^{\mathrm{f}} \, \mathrm{d}\boldsymbol{x} & \forall v^{\mathrm{f}} & \in & H^1(\Omega_{\mathrm{f}}) \\ \int_{\Gamma} u^{\mathrm{f}} \gamma_{\mathbf{n}} v^{\mathrm{m}} \, \mathrm{d}S & - & \int_{\Gamma} u^{\mathrm{m}} \gamma_{\mathbf{n}} v^{\mathrm{m}} \, \mathrm{d}S & = & 0 & \forall v^{\mathrm{m}} & \in & \mathcal{T}(\Omega_{\mathrm{m}}) \end{cases} \qquad (27)$$

Theoretical analysis of (27) on both the continuous and discrete level is based on splitting $u^{\mathrm{f}}, v^{\mathrm{f}} \in H^1(\Omega_{\mathrm{f}})$ as

$$
\begin{aligned}
u^{\mathrm{f}} &= u^{\mathrm{f}}_{\star} + \mu \\
v^{\mathrm{f}} &= v^{\mathrm{f}}_{\star} + \nu
\end{aligned}, \quad u^{\mathrm{f}}_{\star}, v^{\mathrm{f}}_{\star} \in H^1_{\star}(\Omega_{\mathrm{f}}) := \left\{ w \in H^1(\Omega_{\mathrm{f}}) : \int_{\Omega_{\mathrm{f}}} w \, \mathrm{d}\boldsymbol{x} = 0 \right\}, \quad \mu, \nu \in \mathbb{R},
$$

(28)

which leads to the following saddle point problem:

Seek $u^{\mathrm{f}}_{\star} \in H^1_{\star}(\Omega_{\mathrm{f}}), \, u^{\mathrm{m}} \in \mathcal{T}(\Omega_{\mathrm{m}}), \, \mu \in \mathbb{R}$:

$$
\left\{
\begin{array}{rcl}
\int_{\Omega_{\mathrm{f}}} \mathbf{A}\nabla u^{\mathrm{f}}_{\star} \cdot \nabla v^{\mathrm{f}}_{\star} \, \mathrm{d}\boldsymbol{x} \; - \; \int_{\Gamma} \gamma_{\mathbf{n}} u^{\mathrm{m}} \, v^{\mathrm{f}}_{\star} \, \mathrm{d}S & = & \int_{\Omega_{\mathrm{f}}} f \, v^{\mathrm{f}}_{\star} \, \mathrm{d}\boldsymbol{x} \\[2mm]
\int_{\Gamma} u^{\mathrm{f}}_{\star} \, \gamma_{\mathbf{n}} v^{\mathrm{m}} \, \mathrm{d}S \; - \; \int_{\Gamma} u^{\mathrm{m}} \, \gamma_{\mathbf{n}} v^{\mathrm{m}} \, \mathrm{d}S + \int_{\Gamma} \mu \, \gamma_{\mathbf{n}} v^{\mathrm{m}} \, \mathrm{d}S & = & 0 \\[2mm]
- \int_{\Gamma} \gamma_{\mathbf{n}} u^{\mathrm{m}} \, \mathrm{d}S & = & \int_{\Omega_{\mathrm{f}}} f \, \mathrm{d}\boldsymbol{x}
\end{array}
\right.
$$

$\forall v^{\mathrm{f}}_{\star} \in H^1_{\star}(\Omega_{\mathrm{f}}), \quad \forall v^{\mathrm{m}} \in \mathcal{T}(\Omega_{\mathrm{m}})$

(29)

Galerkin discretization of (29) is straightforward: as in section 3.1, we replace $H^1(\Omega_{\mathrm{f}})$ with a Lagrangian finite element space and $\mathcal{T}(\Omega_{\mathrm{m}})$ with a finite-dimensional subspace $\mathcal{T}_n$.

To apply saddle point theory to (29), let us define the following operators:

$$
\mathrm{a}^{\mathrm{DtN}}\left((u^{\mathrm{f}}_{\star}, u^{\mathrm{m}}), (v^{\mathrm{f}}_{\star}, v^{\mathrm{m}})\right) := \int_{\Omega_{\mathrm{f}}} \mathbf{A}\nabla u^{\mathrm{f}}_{\star} \cdot \nabla v^{\mathrm{f}}_{\star} \, \mathrm{d}\boldsymbol{x} - \int_{\Gamma} \gamma_{\mathbf{n}} u^{\mathrm{m}} \, v^{\mathrm{f}}_{\star} \, \mathrm{d}S +
$$

$$
+ \int_{\Gamma} u^{\mathrm{f}}_{\star} \, \gamma_{\mathbf{n}} v^{\mathrm{m}} \, \mathrm{d}S - \int_{\Gamma} u^{\mathrm{m}} \, \gamma_{\mathbf{n}} v^{\mathrm{m}} \, \mathrm{d}S , \qquad \text{(30a)}
$$

$$
\mathrm{b}^{\mathrm{DtN}}(u^{\mathrm{m}}, \mu) := \int_{\Gamma} \gamma_{\mathbf{n}} u^{\mathrm{m}} \, \mu \, \mathrm{d}S . \qquad \text{(30b)}
$$

For $u^{\mathrm{m}} \in \ker \mathrm{b}^{\mathrm{DtN}}$, we have that $\int_{\Gamma} \gamma_{\mathbf{n}} u^{\mathrm{m}} \, \mathrm{d}S = 0$, which implies $\nabla u^{\mathrm{m}}(\mathbf{x}) = \mathcal{O}\left(\|\mathbf{x}\|^{-2}\right)$ for $\|\mathbf{x}\| \to \infty$. As a consequence,

$$
\mathrm{a}^{\mathrm{DtN}}\left((u^{\mathrm{f}}_{\star}, u^{\mathrm{m}}), (u^{\mathrm{f}}_{\star}, u^{\mathrm{m}})\right) = \int_{\Omega_{\mathrm{f}}} \mathbf{A}\nabla u^{\mathrm{f}}_{\star} \cdot \nabla u^{\mathrm{f}}_{\star} \, \mathrm{d}\boldsymbol{x} + \int_{\Omega_{\mathrm{m}}} \|\nabla u^{\mathrm{m}}\|^2 \, \mathrm{d}\boldsymbol{x} . \qquad \text{(31)}
$$

14

This proves the ellipticity on the kernel in both the continuous and discrete settings: the variational problems are uniformly stable.

The inf-sup condition for b^{DtN} of (30b) is trivial considering that $\mu \in \mathbb{R}$ and $\gamma_{\mathbf{n}} u^{\text{m}} \neq 0$ for some $u^{\text{m}} \in \mathcal{T}(\Omega_{\text{m}})$.

3.3. Multi-Field Coupling

We introduce the unknown $\lambda := \gamma_{\mathbf{n}} u^{\text{m}}$ and insert it into (15), while we enforce both the defining equation $\lambda := \gamma_{\mathbf{n}} u^{\text{m}}$ and the transmission condition (14a) in a weak sense. Note that (14a) is an equation connecting traces in $H^{\frac{1}{2}}(\Gamma)$ and therefore it has to be tested with functions in the dual space $H^{-\frac{1}{2}}(\Gamma)$. We end up with:

Seek $u^{\text{f}} \in H^1(\Omega_{\text{f}})$, $u^{\text{m}} \in \mathcal{T}(\Omega_{\text{m}})$, $\lambda \in H^{-\frac{1}{2}}(\Gamma)$:

$$
\begin{cases}
\displaystyle\int_{\Omega_{\text{f}}} \mathbf{A}\,\nabla u^{\text{f}} \cdot \nabla v^{\text{f}}\,\mathrm{d}\boldsymbol{x} & -\displaystyle\int_{\Gamma} \lambda\,v^{\text{f}}\,\mathrm{d}S & = \displaystyle\int_{\Omega_{\text{f}}} f\,v^{\text{f}}\,\mathrm{d}\boldsymbol{x} \\[2ex]
-\displaystyle\int_{\Gamma} \gamma_{\mathbf{n}} u^{\text{m}}\,v^{\text{m}}\,\mathrm{d}S & +\displaystyle\int_{\Gamma} \lambda\,v^{\text{m}}\,\mathrm{d}S & = 0 \\[2ex]
-\displaystyle\int_{\Gamma} u^{\text{f}}\,v_{\lambda}\,\mathrm{d}S + \displaystyle\int_{\Gamma} u^{\text{m}}\,v_{\lambda}\,\mathrm{d}S & & = 0
\end{cases}
$$

$$\forall v^{\text{f}} \in H^1(\Omega_{\text{f}}), \quad \forall v^{\text{m}} \in \mathcal{T}(\Omega_{\text{m}}), \quad \forall v_{\lambda} \in H^{-\frac{1}{2}}(\Gamma) \tag{32}$$

For the Galerkin discretization of (32), we replace $H^1(\Omega_{\text{f}})$ with a Lagrangian finite element space V_n and $\mathcal{T}(\Omega_{\text{m}})$ with a finite-dimensional subspace $\mathcal{T}_n$, as in sections 3.1 and 3.2. For discretizing λ we use the traces of the finite element functions in V_n on the boundary Γ.

To apply saddle point theory to (32), let us consider the left-hand side of (32) and define the following bilinear form:

$$\mathrm{a}^{\text{MF}}\left(\left(u^{\text{f}}, u^{\text{m}}\right), \left(v^{\text{f}}, v^{\text{m}}\right)\right) := \int_{\Omega_{\text{f}}} \mathbf{A}\,\nabla u^{\text{f}} \cdot \nabla v^{\text{f}}\,\mathrm{d}\boldsymbol{x} - \int_{\Gamma} \gamma_{\mathbf{n}} u^{\text{m}}\,v^{\text{m}}\,\mathrm{d}S . \tag{33}$$

Let us also define

$$\mathrm{b}^{\text{MF}}\left(\left(u^{\text{f}}, u^{\text{m}}\right), \lambda\right) := \int_{\Gamma} \left(u^{\text{f}} - u^{\text{m}}\right) \lambda\,\mathrm{d}S . \tag{34}$$

15

We restrict ourselves to $d = 3$ and observe that, in this case,

$$a^{\mathrm{MF}}\left(\left(u^{\mathrm{f}}, u^{\mathrm{m}}\right), \left(u^{\mathrm{f}}, u^{\mathrm{m}}\right)\right) = \int_{\Omega_{\mathrm{f}}} \mathbf{A} \nabla u^{\mathrm{f}} \cdot \nabla u^{\mathrm{f}} \, \mathrm{d}\boldsymbol{x} + \int_{\Omega_{\mathrm{m}}} \left\|\nabla u^{\mathrm{m}}\right\|^2 \, \mathrm{d}\boldsymbol{x} \,. \qquad (35)$$

In the continuous case we have that

$$\ker \mathrm{b}^{\mathrm{MF}} = \left\{ v^{\mathrm{f}} \in H^1\left(\Omega_{\mathrm{f}}\right), \, v^{\mathrm{m}} \in \mathcal{T}\left(\Omega_{\mathrm{m}}\right) : \, v^{\mathrm{f}} = v^{\mathrm{m}} \text{ on } \Gamma \right\} \qquad (36)$$

and ellipticity on the kernel is clear.

In the discrete case, since V_n contains constant functions, the right-hand side of (35) is still a norm on the discrete kernel $\ker_n \mathrm{b}^{\mathrm{MF}}$, which also amounts to ellipticity on the kernel.

The continuous inf-sup condition for b^{MF} is a consequence of the duality of $H^{\frac{1}{2}}\left(\Gamma\right)$ and $H^{-\frac{1}{2}}\left(\Gamma\right)$.

We discuss the discrete inf-sup condition for the concrete case of piecewise linear Lagrangian finite elements on a tetrahedral mesh $\mathcal{M}_{\mathrm{f}}$ of Ω_{f}: $V_n = \mathcal{S}_1^0\left(\mathcal{M}_{\mathrm{f}}\right)$, with

$$\mathcal{S}_1^0\left(\mathcal{M}_{\mathrm{f}}\right) := \{v \in C^0\left(\Omega_{\mathrm{f}}\right) : \, \forall K \in \mathcal{M}_{\mathrm{f}} : \, v|_K\left(\mathbf{x}\right) = \alpha_K + \boldsymbol{\beta}_K \cdot \mathbf{x},$$
$$\alpha_K \in \mathbb{R}, \, \boldsymbol{\beta}_K \in \mathbb{R}^3, \, \mathbf{x} \in K\} \subset H^1\left(\Omega_{\mathrm{f}}\right), \quad \mathcal{M}_{\mathrm{f}} \text{ mesh of } \Omega_{\mathrm{f}} \,. \qquad (37)$$

The $H^{-\frac{1}{2}}$-norm of $\lambda_n \in V_n$ can be expressed as

$$\left\|\lambda_n\right\|_{H^{-\frac{1}{2}}\left(\Gamma\right)} := \sup_{v \in H^{\frac{1}{2}}\left(\Gamma\right)} \frac{\int_{\Gamma} \mathrm{Q}_n v \, \lambda_n \, \mathrm{d}S}{\left\|v\right\|_{H^{\frac{1}{2}}\left(\Gamma\right)}} \leq C \sup_{v \in H^{\frac{1}{2}}\left(\Gamma\right)} \frac{\int_{\Gamma} \mathrm{Q}_n v \, \lambda_n \, \mathrm{d}S}{\left\|\mathrm{Q}_n v\right\|_{H^{\frac{1}{2}}\left(\Gamma\right)}} \,, \qquad (38)$$

where $\mathrm{Q}_n : L^2\left(\Gamma\right) \to V_n|_{\Gamma}$ is the L^2-*orthogonal projection operator* such that, given $u \in L^2\left(\Gamma\right)$,

$$\mathrm{Q}_n u \in V_n|_{\Gamma} : \int_{\Gamma} \left(u - \mathrm{Q}_n u\right) v_n \, \mathrm{d}S = 0 \quad \forall v_n \in V_n \,. \qquad (39)$$

Under mild assumptions on the surface mesh $\mathcal{M}_{\mathrm{f}}|_{\Gamma}$, we have that $\left\|\mathrm{Q}_n u_{\Gamma}\right\|_{H^1\left(\Gamma\right)} \leq C \left\|u_{\Gamma}\right\|_{H^1\left(\Gamma\right)}$ $\forall u_{\Gamma} \in H^1\left(\Gamma\right)$, $C \in \mathbb{R}^+$ independent of V_n [26, 27, 28]. Appealing to interpolation between $L^2\left(\Gamma\right)$ and $H^1\left(\Gamma\right)$, we conclude with

$$\left\|\mathrm{Q}_n u_{\Gamma}\right\|_{H^{\frac{1}{2}}\left(\Gamma\right)} \leq C \left\|u_{\Gamma}\right\|_{H^{\frac{1}{2}}\left(\Gamma\right)} \,. \qquad (40)$$

4. Numerical Experiments

Throughout we use piecewise linear Lagrangian finite elements, i.e. $V_n = \mathcal{S}_1^0(\mathcal{M}_\mathrm{f})$ (see (37)), on triangular/tetrahedral meshes $\mathcal{M}_\mathrm{f}$ of Ω_f.

To study the convergence we employ uniform h-refinement of $\mathcal{M}_\mathrm{f}$ and p-refinement of the Trefftz approximation, in the sense that we increase the number of multipole expansions. The p-refinement of the multipoles is set dependent to the h-refinement of $\mathcal{M}_\mathrm{f}$. Details on this dependence are given for each convergence test.

We monitor the following L^2-errors:

1. The error in the FE domain, which is the relative $L^2(\Omega_\mathrm{f})$-error compared to the reference solution in Ω_f, i.e. $\left\| u - \sum_{i=1}^{N} u(x_i)\varphi_i(x) \right\|_{L^2(\Omega_\mathrm{f})} \Big/ \|u\|_{L^2(\Omega_\mathrm{f})}$, $\varphi_i \in \mathcal{S}_1^0(\mathcal{M}_\mathrm{f})$.

2. The MMP error on the interface, which is the relative $L^2(\Gamma)$-error compared to the reference solution on Γ.

The average between the relative L^2-error for FEM in Ω_f and the relative L^2-error for MMP on Γ is the total relative error of the coupling.

To ignore the impact of numerical integration for FEM, we use a Gaussian quadrature rule that is exact for polynomials of degree 2 (order 3).

Implementation. The code is written in `C++14`, using `C++11` multithreading for parallelization. We use `Eigen` v3.2.10 [29] for linear algebra and `HyDi` [30] for the FEM component. The `PARDISO` v5.0.0 solver [31, 32] provides the sparse LU decomposition to invert the matrices of the coupling, characterized by nontrivial sparsity patterns.

4.1. 2D Poisson's Equation With Exact Solution

We solve $-\triangle u = j$ in $\mathbb{R}^2$, with $|j| = 1.05 \cdot 10^6$ in $\Omega_\star$ and $= 0$ elsewhere. A sample mesh is shown in fig. 4.

Multipole expansions are uniformly positioned on a circle of radius 1 centered in the origin. We only use multipoles up to order 1.

Figure 5 shows the h-refinement convergence plot for the DtN-based approach. Plots obtained with the other approaches look the same. We can clearly identify a quadratic convergence of the FEM and MMP errors. For MMP, the number of multipoles is set to the natural logarithm of the number of vertices of the FEM meshes on the boundary Γ.
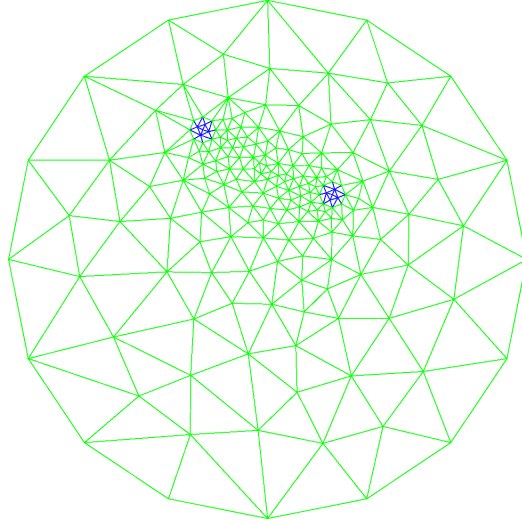
Figure 4: The blue and green meshes cover the FEM domain Ω_{f}. The blue disks of radius 0.1 represent $\Omega_{\star}$, the area where j is nonzero: in one is $= 1.05 \cdot 10^6$, in the other $= -1.05 \cdot 10^6$. They are centered at $(0.5, 0.5)^{\top}$ and $(-0.5, 1)^{\top}$. The green hollow disk is centered in the origin and has radius 2.
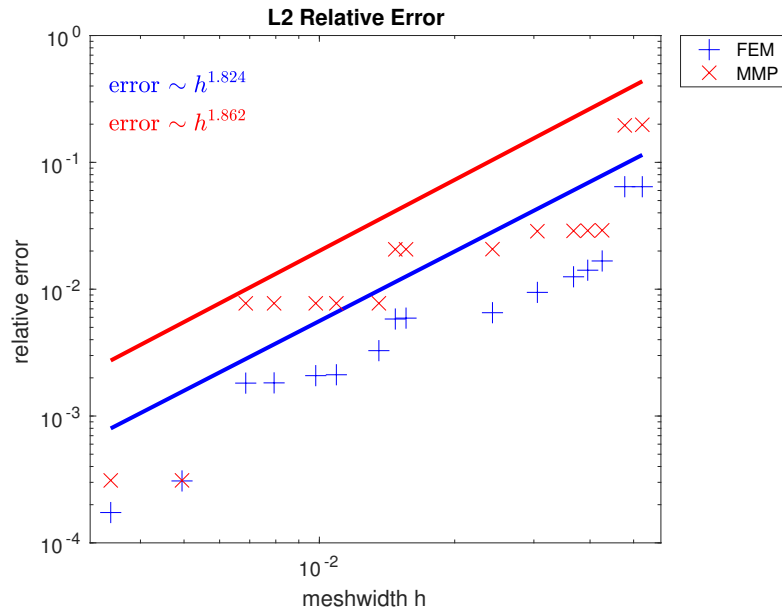

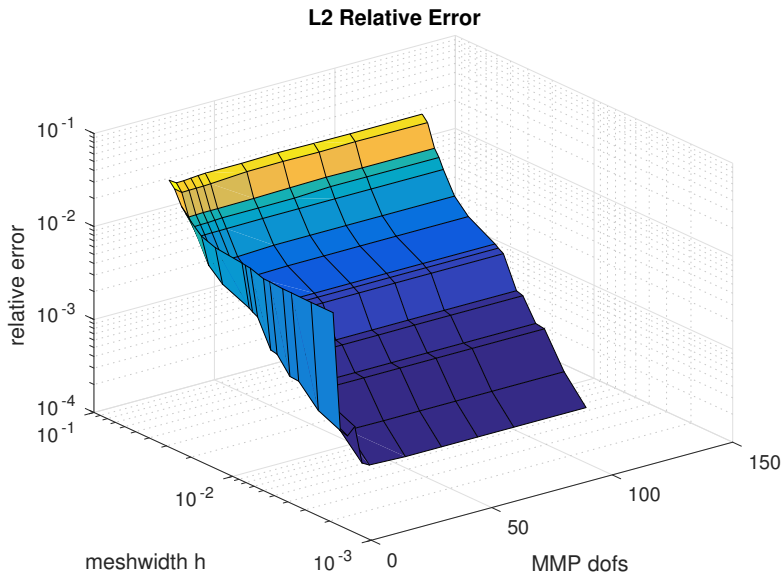Figure 5: h-refinement plot for 2D Poisson with exact solution. Plot obtained with the DtN-based approach.

18

Figure 6: Meshwidth h vs. MMP degrees of freedom for 2D Poisson with exact solution: total relative error. Plot obtained with the DtN-based approach.

Figure 6 shows a surface plot of the total relative L^2-error for the DtN-based approach. Plots obtained with the other approaches look the same. The error decreases with h (algebraic convergence) and is generally independent from the number of multipoles. This is due to the fact that the exact solution is so easy to approximate in the MMP domain that can already be represented by very few multipoles. However, the error also becomes worse with the coarsest meshes and the highest number of multipoles considered: the FEM error dominates.

4.2. 2D Diffusion Problem with Jumping Coefficients

We solve $-\nabla \cdot (\kappa \nabla u) = j$ in $\mathbb{R}^2$, with $\kappa = \frac{1}{10}$, $j = 1.05 \cdot 10^6$ in $\Omega_\star$ and $\kappa = 1$, $j = 0$ elsewhere. $\Omega_\star$ is the U-shaped region displayed in fig. 7: there is no exact solution. As reference we consider the numerical solution provided by a mesh more refined than the most refined mesh of the convergence test.

All types of meshes employed are shown in fig. 7: we consider three examples where the boundary Γ has different positions and shapes.

With Γ at the discontinuities of κ and j, multipoles are uniformly positioned along the skeleton inside Ω_f (see fig. 7a). With an auxiliary Γ, multipoles are uniformly positioned along a line following the skeleton of $\Omega_f \setminus \Omega_\star$,
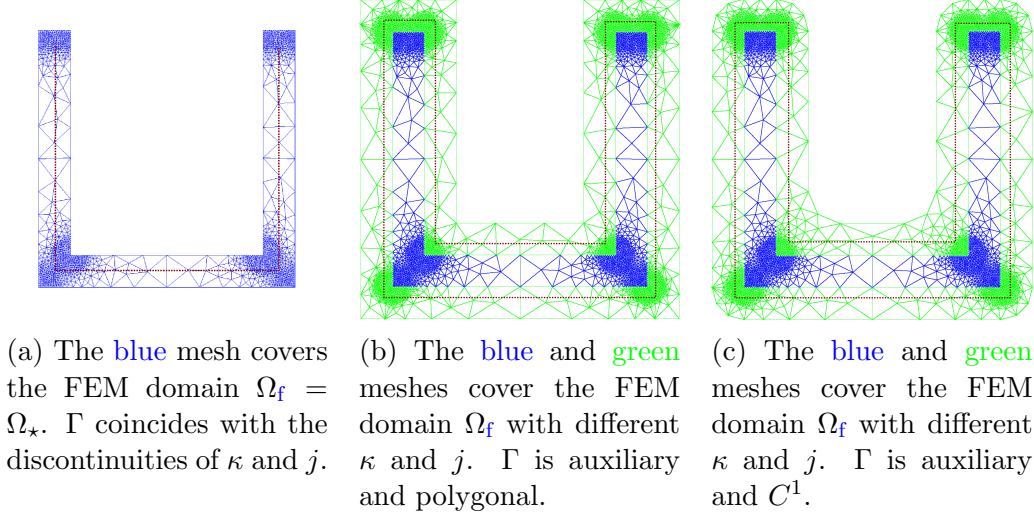
(a) The blue mesh covers the FEM domain $\Omega_f = \Omega_\star$. Γ coincides with the discontinuities of κ and j.

(b) The blue and green meshes cover the FEM domain Ω_f with different κ and j. Γ is auxiliary and polygonal.

(c) The blue and green meshes cover the FEM domain Ω_f with different κ and j. Γ is auxiliary and C^1.

Figure 7: The blue U-shape, which fits into $[0,2]^2$, represents $\Omega_\star$ with $\kappa = \frac{1}{10}$ and $j = 1.05 \cdot 10^6$. The green part of the mesh is characterized by $\kappa = 1$ and $j = 0$. The dotted brown line is the curve along which multipoles are positioned. The local refinement at the corners of the internal square is needed because the solution is not smooth there.

which is positioned at a distance of 0.15 from $\partial\Omega_\star$ (see figs. 7b and 7c). We only use multipoles of order 0 (fundamental solutions of $-\triangle u = 0$).

Given the different boundaries Γ, for a fair comparison the MMP error has not been computed as a boundary error, but on coarser meshes encompassing the area around Ω_f bounded by $[0,4]^2$. The number of multipoles is set to the natural logarithm of the number of vertices of the FEM meshes on the boundary Γ, multiplied by 10.

Figure 8 shows the h-refinement convergence plots for all coupling approaches given Γ at the discontinuities. We can identify an algebraic convergence of the FEM and MMP errors, but with quite different rates depending on the coupling approach.

Figure 9 shows the h-refinement convergence plots for the DtN-based approach given an auxiliary Γ, either with or without corners. Plots obtained with the other approaches look the same. We can clearly identify an algebraic convergence of the FEM and MMP errors.

No surface plot is included. The reason is the lack of an exact solution. Using a numerical solution on a very refined mesh is justifiable for h-refinement. However, a very high number of multipoles does not necessarily lead to a solution that is more accurate, given the ill-conditioning of the
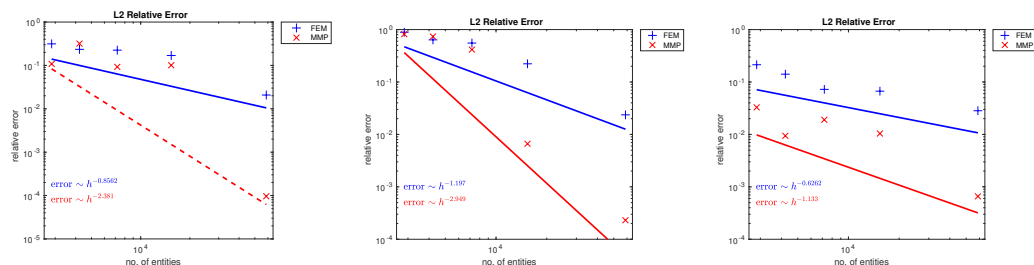
(a) Obtained with the DtN-based approach.

(b) Obtained with the PDE-constr. approach.

(c) Obtained with the multi-field approach.

Figure 8: h-refinement plots for 2D Poisson without exact solution. Γ coincides with the discontinuities of κ and j (see fig. 7a).
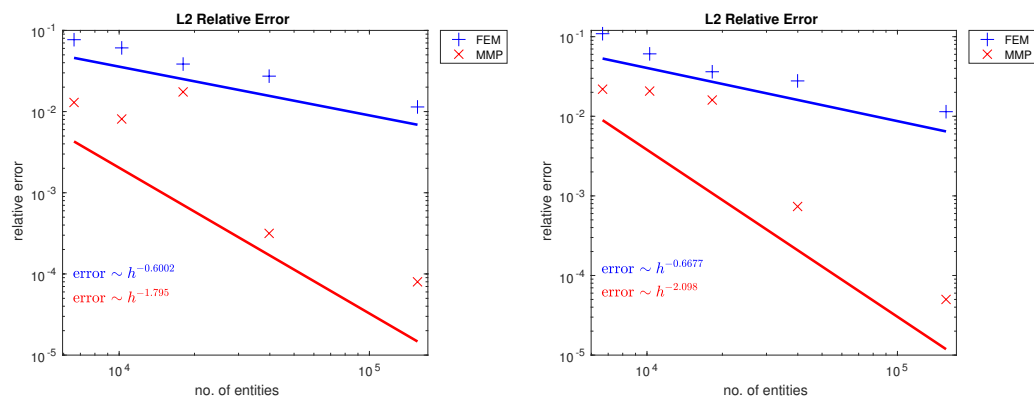
(a) Γ is polygonal (see fig. 7b).

(b) Γ is C^1 (see fig. 7c).

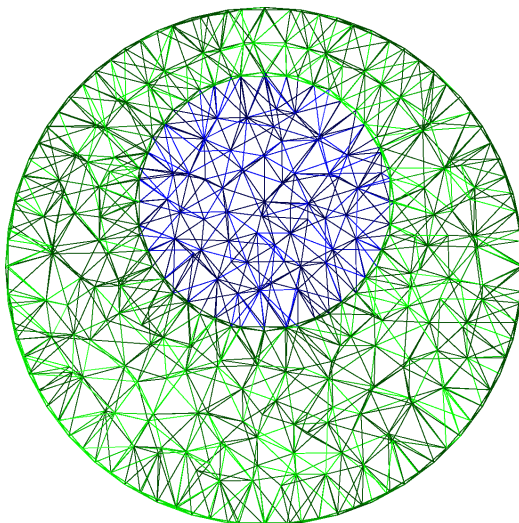Figure 9: h-refinement plots for 2D Poisson without exact solution. Γ is auxiliary. Plots obtained with the DtN-based approach.

21

Figure 10: Cross-section of 3D mesh along the XZ-plane. The blue and green meshes cover the FEM domain Ω_f. The blue sphere of radius 1 represents $\Omega_\star$, the volume where $q \neq 0$. It is centered at $(0, 0, 0.5)^\top$. The green hollow sphere is centered in the origin and has radius 2.

corresponding block in the linear system for the coupling (see section 1.1).

4.3. 3D Poisson's Equation With Exact Solution

We solve $-\triangle u = q$ in $\mathbb{R}^2$, with $q = \frac{3}{4\pi}$ in $\Omega_\star$ and $= 0$ elsewhere. A sample mesh is shown in fig. 10.

Multipole expansions are uniformly positioned on a circle of radius 1 centered in the origin and lying on the XY-plane. We only use multipoles up to order 1.

Figure 11 shows the h-refinement convergence plot for the DtN-based approach. Plots obtained with the other approaches look the same. We can clearly identify an algebraic convergence of the FEM and MMP errors. For MMP, the number of multipole expansions is set to the natural logarithm of the number of vertices of the FEM meshes on the boundary Γ.

Figure 12 shows the surface plot of the total relative L^2-error for the DtN-based approach. Plots obtained with the other approaches look the same. The error decreases with h (algebraic convergence) and is generally independent from the number of multipoles.
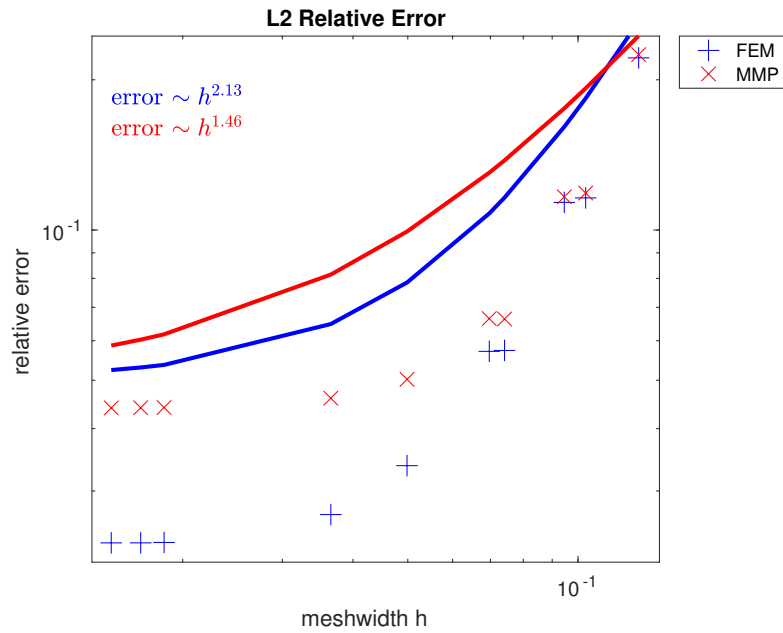
Figure 11: h-refinement plot for 3D Poisson with exact solution. Plot obtained with the DtN-based approach.
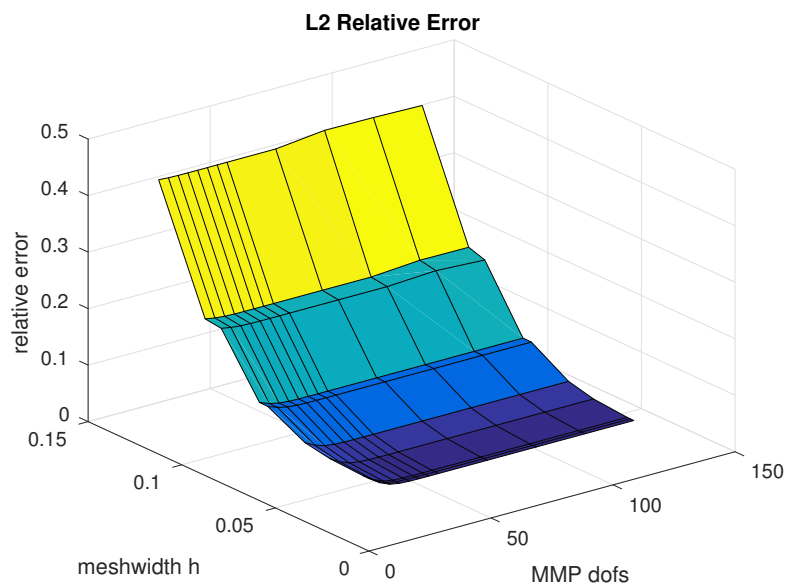

Figure 12: Meshwidth h vs. MMP degrees of freedom for 3D Poisson with exact solution: total relative error. Plot obtained with the DtN-based approach.

23

5. Conclusions

Among the three coupling approaches presented in sections 3.1 to 3.3, none is clearly superior. We recommend the DtN-based approach thanks to its complete convergence theory and good practical performance. We point out that in this work several important issues have not been addressed: solving the linear systems (iteratively), ill-conditioning when using many or high-order multipoles, and vector Maxwell's equations.

6. Acknowledgements

[1] W. McLean, Strongly Elliptic Systems and Boundary Integral Equations, Cambridge University Press, 2000.

[2] R. Hiptmair, A. Moiola, I. Perugia, A Survey of Trefftz Methods for the Helmholtz Equation, Springer International Publishing, Cham, 2016, pp. 237–279. `doi:10.1007/978-3-319-41640-3_8`.
URL `https://doi.org/10.1007/978-3-319-41640-3_8`

[3] C. Chen, S. Reutskiy, V. Rozov, The method of the fundamental solutions and its modifications for electromagnetic field problems, Computer Assisted Methods in Engineering and Science 16 (1) (2017) 21–33.
URL `http://cames.ippt.gov.pl/index.php/cames/article/view/161`

[4] T. Betcke, L. N. Trefethen, Reviving the Method of Particular Solutions, SIAM Review 47 (3) (2005) 469–491. `arXiv:https://doi.org/10.1137/S0036144503437336`, `doi:10.1137/S0036144503437336`.
URL `https://doi.org/10.1137/S0036144503437336`

[5] D. I. Kaklamani, H. T. Anastassiu, Aspects of the Method of Auxiliary Sources (MAS) in computational electromagnetics, IEEE Antennas and Propagation Magazine 44 (3) (2002) 48–64. `doi:10.1109/MAP.2002.1028734`.

[6] Y.-S. Smyrlis, Applicability and Applications of the Method of Fundamental Solutions, Mathematics of Computation 78 (267) (2009) 1399–1434.
URL http://www.jstor.org/stable/40234665

[7] M. Katsurada, Charge simulation method using exterior mapping functions, Japan Journal of Industrial and Applied Mathematics 11 (1) (1994) 47. doi:10.1007/BF03167213.
URL https://doi.org/10.1007/BF03167213

[8] M. Katsurada, H. Okamoto, The collocation points of the fundamental solution method for the potential problem, Computers & Mathematics with Applications 31 (1) (1996) 123 – 137. doi:https://doi.org/10.1016/0898-1221(95)00186-3.
URL http://www.sciencedirect.com/science/article/pii/0898122195001863

[9] K. Sakakibara, Analysis of the dipole simulation method for two-dimensional dirichlet problems in jordan regions with analytic boundaries, BIT Numerical Mathematics 56 (4) (2016) 1369–1400. doi:10.1007/s10543-016-0605-1.
URL https://doi.org/10.1007/s10543-016-0605-1

[10] Y. A. Eremin, A. G. Sveshnikov, A Computer Technology for the Discrete Source Method in Scattering Problems, Computational Mathematics and Modeling 14 (1) (2003) 16–25. doi:10.1023/A:1022069632726.
URL https://doi.org/10.1023/A:1022069632726

[11] C. J. Gittelson, R. Hiptmair, I. Perugia, Plane wave discontinuous Galerkin methods: Analysis of the h-version, M2AN Math. Model. Numer. Anal. 43 (2) (2009) 297–331. doi:10.1051/m2an/2009002.
URL http://dx.doi.org/10.1051/m2an/2009002

[12] R. Hiptmair, A. Moiola, I. Perugia, Plane wave discontinuous Galerkin methods for the 2D Helmholtz equation: Analysis of the p-version, SIAM Journal on Numerical Analysis 49 (1) (2011) 264–284. arXiv:https://doi.org/10.1137/090761057, doi:10.1137/090761057.
URL https://doi.org/10.1137/090761057

[13] R. Hiptmair, A. Moiola, I. Perugia, Stability results for the time-harmonic Maxwell equations with impedance boundary conditions, Mathematical Models and Methods in Applied Sciences 21 (11) (2011) 2263–2287. `arXiv:http://www.worldscientific.com/doi/pdf/10.1142/S021820251100574X`, `doi:10.1142/S021820251100574X`.
URL `http://www.worldscientific.com/doi/abs/10.1142/S021820251100574X`

[14] R. Hiptmair, A. Moiola, I. Perugia, Plane Wave Discontinuous Galerkin Methods: Exponential Convergence of the hp-Version, Foundations of Computational Mathematics 16 (3) (2016) 637–675. `doi:10.1007/s10208-015-9260-1`.
URL `https://doi.org/10.1007/s10208-015-9260-1`

[15] R. Hiptmair, A. Moiola, I. Perugia, Error analysis of Trefftz-discontinuous Galerkin methods for the time-harmonic Maxwell equations, Mathematics of Computation 82 (281) (2013) 247–268. `doi:10.1090/S0025-5718-2012-02627-5`.

[16] A. Barnett, T. Betcke, Stability and convergence of the method of fundamental solutions for Helmholtz problems on analytic domains, Journal of Computational Physics 227 (14) (2008) 7003 – 7026. `doi:https://doi.org/10.1016/j.jcp.2008.04.008`.
URL `http://www.sciencedirect.com/science/article/pii/S0021999108002106`

[17] A. H. Barnett, T. Betcke, An Exponentially Convergent Nonpolynomial Finite Element Method for Time-Harmonic Scattering from Polygons, SIAM Journal on Scientific Computing 32 (3) (2010) 1417–1441. `arXiv:https://doi.org/10.1137/090768667`, `doi:10.1137/090768667`.
URL `https://doi.org/10.1137/090768667`

[18] P. R. S. Antunes, A numerical algorithm to reduce the ill conditioning in meshless methods for the Helmholtz equation, submitted (2017).

[19] J. Smajic, C. Hafner, J. Leuthold, Coupled FEM–MMP for Computational Electromagnetics, IEEE Transactions on Magnetics PP (99) (2015) 1–1. `doi:10.1109/TMAG.2015.2475241`.

[20] C. Hafner, Beiträge zur Berechnung der Ausbreitung elektromagnetischer Wellen in zylindrischen Strukturen mit Hilfe des "Point-Matching"-Verfahrens, ETH Dissertation 6683, ETH Zurich, Switzerland (1980).

[21] G. Mie, Elektrische Wellen an zwei parallelen Drähten, Annalen der Physik 307 (1900) 201–249. `doi:10.1002/andp.19003070602`.

[22] I. N. Vekua, New methods for solving elliptic equations, North Holland Publishing Company, 1967.

[23] A. Moiola, Trefftz-Discontinuous Galerkin Methods for Time-Harmonic Wave Problems, PhD dissertation, Seminar for Applied Mathematics, ETH Zurich (2011). `doi:10.3929/ethz-a-006698757`.

[24] P. Monk, Finite Element Methods for Maxwell's Equations, Clarendon Press, 2003.

[25] D. Braess, Finite Elements: Theory, Fast Solvers, and Applications in Solid Mechanics, 3rd Edition, Cambridge University Press, 2007. `doi:10.1017/CBO9780511618635`.

[26] J. H. Bramble, J. E. Pasciak, O. Steinbach, On the Stability of the L^2 Projection in $H^1(\Omega)$, Mathematics of Computation 71 (237) (2002) 147–156.
URL `http://www.jstor.org/stable/2698864`

[27] R. E. Bank, H. Yserentant, On the H^1-stability of the L^2-projection onto finite element spaces, Numerische Mathematik 126 (2) (2014) 361–381. `doi:10.1007/s00211-013-0562-4`.
URL `https://doi.org/10.1007/s00211-013-0562-4`

[28] C. Carstensen, Merging the Bramble-Pasciak-Steinbach and the Crouzeix-Thomée Criterion for H^1-Stability of the L^2-Projection onto Finite Element Spaces, Mathematics of Computation 71 (237) (2002) 157–163.
URL `http://www.jstor.org/stable/2698865`

[29] G. Guennebaud, B. Jacob, et al., Eigen v3, http://eigen.tuxfamily.org (2010).

[30] R. Casagrande, C. Winkelmann, et al., Hybrid Discontinuous Finite Elements for Power Devices, ABB Corporate Research Center (2016).

[31] C. G. Petra, O. Schenk, M. Lubin, K. Gärtner, An augmented incomplete factorization approach for computing the Schur complement in stochastic optimization, SIAM Journal on Scientific Computing 36 (2) (2014) C139–C162.

[32] C. G. Petra, O. Schenk, M. Anitescu, Real-time stochastic optimization of complex energy systems on high-performance computers, IEEE Computing in Science & Engineering 16 (5) (2014) 32–42.